

Green Chemistry

Accepted Manuscript



This is an *Accepted Manuscript*, which has been through the Royal Society of Chemistry peer review process and has been accepted for publication.

Accepted Manuscripts are published online shortly after acceptance, before technical editing, formatting and proof reading. Using this free service, authors can make their results available to the community, in citable form, before we publish the edited article. We will replace this *Accepted Manuscript* with the edited and formatted *Advance Article* as soon as it is available.

You can find more information about *Accepted Manuscripts* in the [Information for Authors](#).

Please note that technical editing may introduce minor changes to the text and/or graphics, which may alter content. The journal's standard [Terms & Conditions](#) and the [Ethical guidelines](#) still apply. In no event shall the Royal Society of Chemistry be held responsible for any errors or omissions in this *Accepted Manuscript* or any consequences arising from the use of any information it contains.

Efficient and simple reactive milling preparation of photocatalytically active porous ZnO nanostructures using biomass derived polysaccharides

Matteo Francavilla^{a,b}, Antonio Pineda^c, Antonio A. Romero^c, Juan Carlos Colmenares^d, Carolina Vargas^c, Massimo Monteleone^a, Rafael Luque^{*c}

^aSTAR-Agroenergy Research Group, University of Foggia, via Gramsci 89/91, 71121, Foggia (ITALY). E-mail: matteo.francavilla@unifg.it; Tel: +39 3403927680.

^bInstitute of Marine Science, Nat. Research Council, via Pola 4, 71010 Lesina (ITALY)

^cDepartamento de Química Organica, Universidad de Córdoba, Campus de Rabanales, Edificio Marie Curie, Ctra Nnal IV-A, Km 396, E14014, Córdoba, Spain. E-mail: g62alsor@uco.es; Fax: +34 957212066; Tel: +34 957211050

^dInstitute of Physical Chemistry, Polish Academy of Sciences, ul. Kasprzaka 44/52, 01-224 Warsaw, Poland

^eDepartamento de Tecnología Química, Univ. Rey Juan Carlos, Mostoles, Madrid

Abstract

ZnO nanocrystals of different shapes and sizes have been synthesized using an innovative, simple and efficient dry reactive milling methodology using Zn(NO₃)₂ and various polysaccharides as sacrificial templates. Optimum results were achieved using extracted agar from the red seaweed *Gracilaria gracilis*. Upon template removal after calcination at 600°C, the protocol gave rise to a range of porous metal oxide nanomaterials of different shapes and nanoparticle sizes which were found to have excellent photocatalytic properties in aqueous phenol degradation as compared to commercial P25 Evonik titania.

Keywords: ZnO, nanocrystals, macroalgae, polysaccharides, reactive milling, photocatalysis sacrificial templating.

Introduction

Nature inspires scientists to devise smart and innovative approaches that can mimic its miniaturisation and efficiency in the production of energy, biometabolites and materials. An advanced degree of innovation in research can therefore be introduced by designing processes with natural resources from a fundamental and rational understanding.^{1,2}

Nanomaterials because of their unique size-dependent properties and small sizes have a great potential for commercial applications that can improve human lives through important applications including biomedical devices, electronics, catalysis, information technologies, food packaging and preservation, personal care products, as well as environmental technologies.³ Nano-scaled materials, including ZnO nanocrystals, can be synthesized by a variety of methods some of them may be potentially harmful to either the environment or human health. Nevertheless, more versatile and innovative procedures are required for a simplified synthesis of ZnO nanoparticles with variable particle sizes and enhanced electrical and optical properties in order to find suitable applications in various fields (e.g. dye-sensitized solar cells, photocatalysis).

An interesting and highly practically successful approach to ZnO nanomaterials synthesis, due to the possibility to control size, size-dispersion and crystallinity, involves the decomposition of organometallic precursors in a coordinating solvent under high temperatures.^{4,5} However, these methodologies are rather complex in terms of laboratory equipment required, making use of expensive reactants and tedious workup for nanocrystals isolation to achieve fairly pure nanocrystals.

Comparatively, alternative ZnO nanocrystal synthesis protocols have been based on the hydrolysis of zinc salts. An original method based in the addition of LiOH to an ethanolic zinc acetate solution subsequently modified introducing an aging step of very small ZnO nuclei under different temperature or water content conditions.^{6,7}

Other procedures of ZnO nanocrystals synthesis consist in the hydrolysis of zinc alkoxides. Carnes *et al.* reported a method where diethylzinc, tert-butyl alcohol, ethanol and water were involved.⁸ Particle size of ZnO nanocrystals obtained by this method was within the 3-5 nm range. Larger spherical particles were formed as a result of the aggregation of these crystals, developing a porous structure with a particular high surface area.

Electrochemical routes have also been comparably developed for the synthesis of ZnO nanoparticles. An initial electrochemically deposition of zinc metal is followed by an oxidation in an appropriate solution. Size-selective could lead to ZnO nanocrystals between 1.5 and 10 nm diameter. In addition, ZnO films of 10-40 nm in thickness have also been prepared by deposition of higher amounts of zinc metal.⁹

Another relevant methodology to synthesize nanostructured materials involves the utilisation of soft materials as templates (soft templates).¹⁰ Typically, soft templates include macro and microemulsions, micelles or vesicles, and some polymers as well as biological molecular assemblies. Surfactant molecules that in aqueous solution can self assemble to form micelles and vesicles have been used as soft template to prepare ZnO. Cong and Yu reported an interesting method for synthesis of hollow spheres of hybrid ZnO-dye.¹¹ The hybrid ZnO-dye hollow spheres were found to have interesting optical and electronic properties.

Ammonia-catalyzed hydrolysis of zinc dibutoxide in non-ionic reversed micelles was reported as example of the utilization of reverse micelles as templates.¹⁰ Hexagonal

single crystals were observed in all micelle regions and particle size of ZnO was controlled by both solubilised states of water and the size of the micellar droplets but independent of zinc dibutoxide.

Imidazolium tetrafluoroborate ionic liquids in a solvothermal reaction system have also been proposed as soft template for synthesis of spheres and hollow spheres of ZnO with tunable nanostructures.¹² In this case spheres with diameters in the 1 to 2.5 μm range comprising 20 nm diameter nanorods could be obtained. ZnO nanostructures were also prepared by decomposing precursor nanoparticles in NaCl nonaqueous ionic liquid, in which the precursor $\text{Zn}_5(\text{CO}_3)_2(\text{OH})_6$ nanoparticles were first prepared by a one-step, solid state reaction and ground with both NaCl and surfactant nonyl phenyl ether (9) NP-9 or only in NaCl, followed by heating at 850°C for 2 h.¹³ Hexagonal nanoplates were synthesized with an interplanar spacing of ca. 0.28 nm and nanowires (30-60 nm diameter).

With regards to the use of polymers as templates, a polymer-assisted control of particle morphology and particle size of zinc oxide precipitated from aqueous solution was recently reported by Taubert *et al.*¹⁴ Different diblock copolymers were employed to control ZnO nanoparticle morphologies, as well as sizes and size distributions. Hexagonal prismatic particles were observed when water-soluble poly(ethylene oxide-block-methacrylic acid) was used, with variable sizes and size distributions depending on the level of blocks polymerization. Narrow size distributions were obtained regardless of polymerization extension, in case of poly(ethylene oxide-block-styrene sulfonic acid) used as copolymers presenting different particle shape.¹⁴

However, the above mentioned nanomaterials templating can be affected by major drawbacks including high cost of the synthesis and significant environmental impact.¹⁵ Therefore, cost efficiency and environmental sustainability are considered an

intriguing challenge for next future. In this respect, the use of natural, renewable, cheap and abundant template materials (e.g. biopolymers) can be highly attractive to prepare nanostructured materials on a large scale and in a “green” way.¹⁵ Biopolymers including cellulose,¹⁶ starch,¹⁷⁻²⁰ chitosan,²¹⁻²⁴ agarose²⁵⁻²⁸ and alginate^{29,30} have been utilised as sacrificial soft templates to generate metal oxide nanoparticles. The advantages of using these materials as templates include a simple synthetic procedure, generally mild reaction conditions, easy removal, and easy scale-up.³¹ Recently, a biomimetic method to grow crystalline ZnO nanowires employed genetically-modified collagen triple helix peptide nanowires as soft biotemplate. In this case, the diameter and length of nanowires could be controlled by the number of amino acid residues in the triple helix, controllable with recombinant technology.³²

To the best of our knowledge, the use of biopolymers (e.g. polysaccharides) in the solid state as sacrificial templates for the development of nanocrystalline materials via reactive solid state milling has not been reported to date. Moreover, in the light of the growing concern regarding the pollution of the environmental and the need to decrease waste formed during chemical processes, ball milling has emerged as one alternative to the conventional chemical protocols being able to provide effective syntheses with significantly reduced energy consumption.

Following our recent research endeavours to the synthesis of *benign by design* porous nanomaterials using a novel mechanochemical protocol based on solid state grinding of metal precursors and pre-formed supports³³, herein we report a simple methodology for the preparation of porous ZnO nanocrystals with different shapes and sizes by solid state grinding of a zinc precursor [Zn(NO₃)₂] with polysaccharides including a biomass-derived agar extracted from macroalgae³¹ followed by thermal decomposition in the absence of any solvent or hazardous/expensive reagent.

Experimental

Materials preparation

The preparation of bio-templated ZnO nanocrystals was carried out using a ball milling protocol similar to that previously reported by the group. In a typical experiment, the desired quantity of zinc precursor [typically $\text{Zn}(\text{NO}_3)_2 \cdot 6\text{H}_2\text{O}$] was milled with a certain quantity of polysaccharide from 1:1 to 1:10 zinc precursor/polysaccharide w/w ratios in a 125 mL stainless steel recipient of a Retsch-PM100 planetary ball mill at 350 rpm for 30 min (optimized conditions). 18 stainless steel balls of 1 cm diameter were employed. Upon milling, the slightly coloured solid was directly transferred to a ceramic vessel and subsequently calcined in air at 600°C for 3 h. Calcination temperature was selected based on thermal decomposition studies which indicated most organics were removed from the material after 500°C (see TG/DTA experiments and discussion). Samples were denoted as ZnO_{XX} Y:Y w/w in which XX stands for the initials of the utilized polysaccharide as sacrificial template (e.g. AA for alginic acid; ST for starch; AG for extracted macroalgal agar) and Y:Y is the weight to weight ratio of Zn precursor/polysaccharide (see Table 1 for full details).

In the particular case of the macroalgal extracted agar, the polysaccharide was previously extracted from the red seaweed *Gracilaria gracilis* using a previously reported microwave-assisted extraction (MAE).³⁴ Briefly, 1 gram of dried sample was transferred to a teflon extraction vessel of a Ethos 1 (Microwave Accelerated Reaction System for Extraction and Digestion, Milestone, USA) containing 40 mL distilled water; then the vessel was closed upon introduction of a fiber optic probe to measure the

temperature in the systems. The operational parameters employed in the MAE apparatus were the following: magnetron power 100%, ramp temperature time, 10 min. During operation, both temperature and pressure were monitored in a single vessel (control vessel). The temperature programme used for the extraction was 100°C for 10 min. After the extraction, the vessels were opened still warm because of the agar gelling properties. The mixture was filtered using paper filter under vacuum at 70°C. The filtrate was held at room temperature for gel formation, and the gelled material was then frozen in the freezer at -15°C overnight to obtain the native extracted agar (ex. agar). Upon extraction and isolation, the agar was identically utilized in the bio-templating methodology with respect to pure starch and alginic acid.

Materials characterisation

XRD patterns were recorded on a Siemens D5000 diffractometer with CuK α ($\lambda=1.5418 \text{ \AA}$), over a 2θ range from 5 to 80°, using a step size of 0.01° and a counting time per step of 20 s.

Nitrogen adsorption measurements were carried out at 77.4 K using an ASAP 2000 volumetric adsorption analyzer from Micromeritics. The samples were outgassed 24 h at 150°C under vacuum ($p < 10^{-2} \text{ Pa}$) and subsequently analysed. The linear part of the BET equation (relative pressure between 0.05 and 0.30) was used for the determination of the specific surface area. D_{BJH} = mean pore size diameter; V_{BJH} = Pore volumes. The pore size distribution was calculated from the adsorption branch of the N₂ physisorption isotherms and the Barret-Joyner-Halenda (BJH) formula. The cumulative pore volume V_{BJH} was obtained from the pore size distribution (PSD) curve.

The size and morphology of carbonaceous materials were investigated using a Electron Microscopy. Scanning Electron Microscopy (SEM) and elemental analysis

were recorded on a JEOL 173 JSM-6300 Scanning Microscope with energy dispersive X-ray analysis (EDX) at 20 kV. Samples were coated with Au/Pd on a high resolution sputtering SC7640 instrument at a sputtering rate of 1.5 kV per minute, up to 7 nm thickness. Transmission Electron Micrographs (TEM) were recorded on a JEOL JEM-2010HR instrument operated at 300 kV. Samples were suspended in ethanol and deposited straightaway on a copper grid prior to analysis.

XPS measurements were performed in a ultra high vacuum (UHV) multipurpose surface analysis system (SpecsTM model, Germany) operating at pressures $<10^{-10}$ mbar using a conventional X-ray source (XR-50, Specs, Mg K α , 1253.6 eV) in a “stop-and-go” mode to reduce potential damage due to sample irradiation. The survey and detailed Fe and Cu high-resolution spectra (pass energy 25 and 10 eV, step size 1 and 0.1 eV, respectively) were recorded at room temperature with a Phoibos 150-MCD energy analyser. Powdered samples were deposited on a sample holder using double-sided adhesive tape and subsequently evacuated under vacuum ($<10^{-6}$ Torr) overnight. Eventually, the sample holder containing the degassed sample was transferred to the analysis chamber for XPS studies. Binding energies were referenced 190 to the C1s line at 284.6 eV from adventitious carbon. Deconvolution curves for the XPS spectra were obtained using software supplied by the spectrometer manufacturer.

Photocatalytic experiments

Photocatalytic reactions were performed in a Pyrex cylindrical double-walled immersion well reactor with a total volume of 450 mL. The bath reactor was magnetically stirred to obtain a homogeneous suspension of the catalyst. A medium pressure 125 W mercury lamp ($\lambda_{\text{max}} = 365$ nm), supplied by Photochemical Reactors

Ltd. (Model RQ 3010) was placed inside the glass immersion well as light irradiation source. The reaction temperature was set at 30°C.

Phenol solution (50 ppm) was prepared in Milli-Q water. Experiments were conducted from 150 mL of the mother solution and 1 g L⁻¹ of catalyst concentration was used. All reactions were carried out under ambient air (no oxygen bubbling conditions). Approx. 2 mL of samples were periodically taken from the photoreactor at specified times of reaction and filtered through 0.2 µm, 25 mm nylon filters in order to remove the photocatalyst prior to analysis. Phenol degradation was measured, after external standard calibration, by HPLC (Waters HPLC Model 590 pump), equipped with a PDA detector. Separation was performed on a XBridge™ C18 5 µm 4.6 × 150 mm column provided by Waters. The mobile phase was Milli-Q water/methanol (65:35 v/v) mixture with 0.1% of CF₃COOH at a flow rate of 1 mL min⁻¹. The injection volume was 10 µL. Blank experiments were performed in the dark as well as with illumination in the absence of photocatalyst, without observable change in the initial concentration of phenol in both cases.

The degradation rate can be expressed as first-order with respect to phenol concentration:

$$r = \frac{-dC}{dt} = k_{app} * C \quad (1)$$

where k_{app} is the apparent rate constant of a pseudo first order reaction.

The percentage of phenol degradation (D%) was calculated as follows:

$$D\% = \frac{C_0 - C}{C_0} * 100 \quad (2)$$

Results and discussion

Prior to optimisation of synthesis conditions, various Zn precursors were investigated as well as a range of polysaccharides. The selection of Zn(NO₃)₂ was

justified on the basis of preliminary milling experiments showing that non porous amorphous ZnO materials were achieved using different precursors (e.g. ZnCl₂, Zn(CH₃COO)₂·2H₂O) under identical synthesis conditions to those detailed in all experiments from this work (Table 1, ESI, S_{BET} D_{BJH} and V_{BJH} of ZnO crystals from ZnCl₂ were not determined). Results seemed to point out to a better hydrolysis of the metal precursor under the investigated conditions as previously reported.³³ Optimisation of milling conditions also indicated that materials prepared at very short milling times (under 30 min) and low or high milling speed (<300 or over 500 rpm) provided non porous low crystalline materials (see ESI, ZnO 1:2 alginic acid harsh milling conditions).

In view of this set of preliminary experiments, selected milling conditions included the use of Zn(NO₃)₂ as precursor (which provided porous materials and reduced NP sizes as compared to those of other Zn precursors including ZnCl₂ and Zn acetate, Table 1), 350 rpm as optimum speed and 30 min milling. From here, various polysaccharides (e.g. starch, alginic acid and a naturally extracted agar from the red seaweed *Gracilaria gracilis*) and metal precursor/polysaccharide ratios were investigated for the development of ZnO nanomaterials. Textural properties of key synthesized materials have been summarized in Tables 2 and 3 (see also ESI). Initially, varying Zn precursor/polysaccharide ratios were investigated for a particular polysaccharide. Results in Table 2 pointed out that the direct calcination of the Zn precursor either without (ZnO_C) or with milling (ZnO-BMc) gave essentially ZnO non porous materials.

Table 1 Textural properties of synthesized ZnO nanomaterials using different Zn precursors and Alginic acid (AA)

Material	Synthesis conditions	$S_{\text{BET}}^{\text{a}}$ (m^2/g)	$D_{\text{BJH}}^{\text{b}}$ (nm)	$V_{\text{BJH}}^{\text{c}}$ (ml/g)	NP size (XRD/TEM) ^d
ZnO _{AA} 1:2 w/w	4 g Zn (NO ₃) ₂ , 8 g AA, 350 rpm, 30 min	11	<2	0.14	18/20
ZnO _{AA} 1:2 w/w	4 g ZnCl ₂ , 8 g AA, 350 rpm, 30 min	-	-	-	49/-
ZnO _{AA} 1:2 w/w	4 g Zn(Ac) ₂ , 8 g AA, 350 rpm, 30 min	<10	<2	0.09	38/-

^a S_{BET} : specific surface area was calculated by the Brunauer-Emmett-Teller (BET) equation; ^b D_{BJH} : mean pore size diameter was calculated by the Barret-Joyner Halenda (BJH) equation; ^c V_{BJH} : pore volumes were calculated by the Barret-Joyner Halenda (BJH) equation; ^dXRD NP sizes were calculated by the Scherrer equation. TEM NP sizes were worked out from TEM images averaging 15-20 particles.

Comparatively, the use of alginic acid as bio-template provided interesting essentially microporous ZnO nanocrystalline materials with enhanced porosities at increasingly larger quantities of polysaccharide up to a certain extent (Table 2, ZnO_{AA} 1:1 to 1:16 mass ratios). In spite of a slight increase in surface area (from 11 to 16 $\text{m}^2 \text{g}^{-1}$), a further increase from 1:2 Zn precursor/alginate mass ratio did not however entail any significant improvement in terms of textural properties. Structural properties (e.g. crystallinity) were compromised under excessive polysaccharide content (Fig. 1). Based on textural and structural properties, a 1:2 mass ratio was therefore selected as optimum, minimizing quantities of the sacrificial biotemplate, to carry out further experiments. Of note the use of different polysaccharides (e.g. starch - ST, extracted agar from algae - AG) provided similar findings to those included in Table 2 for alginic acid (AA).

Table 2 Textural properties of synthesized ZnO nanocrystals from this work

Material	Synthesis conditions	$S_{\text{BET}}^{\text{a}}$ (m^2/g)	$D_{\text{BJH}}^{\text{b}}$ (nm)	$V_{\text{BJH}}^{\text{c}}$ (ml/g)	NP size (XRD/TEM) ^d
ZnO _C	Direct calcination of Zn(NO ₃) ₂ ·6H ₂ O (no milling)	-	-	-	33/40
ZnO-BMc	Zn(NO ₃) ₂ , no polysaccharide 350 rpm, 30 min	-	-	-	-
ZnO _{AA} 1:1 w/w	4 g Zn (NO ₃) ₂ 4 g AA 350 rpm, 30 min	<10	<2	0.08	39
ZnO _{AA} 1:2 w/w	4 g Zn (NO ₃) ₂ 8 g AA 350 rpm, 30 min	11	<2	0.14	18/20
ZnO _{AA} 1:4 w/w	2 g Zn (NO ₃) ₂ 8 g AA 350 rpm, 30 min	13	<2	0.13	42/45
ZnO _{AA} 1:8 w/w	0.56 g Zn (NO ₃) ₂ 4.5 g AA 350 rpm, 30 min	16	<2	0.14	26/32
ZnO _{AA} 1:16 w/w	0.56 g Zn (NO ₃) ₂ 9 g AA 350 rpm, 30 min	14	<2	0.11	33/35

^a S_{BET} : specific surface area was calculated by the Brunauer-Emmett-Teller (BET) equation; ^b D_{BJH} : mean pore size diameter was calculated by the Barret-Joyner Halenda (BJH) equation; ^c V_{BJH} : pore volumes were calculated by the Barret-Joyner Halenda (BJH) equation; ^dXRD NP sizes were calculated by the Scherrer equation. TEM NP sizes were worked out from TEM images averaging 15-20 particles.

Table 3 Comparison between ZnO nanomaterials synthesized from different polysaccharides: alginic acid (AA); starch (ST); extracted agar from algae-(AG).

Material	Synthesis conditions	$S_{\text{BET}}^{\text{a}}$ (m^2/g)	$D_{\text{BJH}}^{\text{b}}$ (nm)	$V_{\text{BJH}}^{\text{c}}$ (ml/g)	NP size (XRD/TEM) ^d
ZnO-BMc	Zn(NO ₃) ₂ no polysaccharide, 350 rpm, 30 min	-	-	-	-

ZnO _{AA} 1:2 w/w	4 g Zn(NO ₃) ₂ 8 g AA 350 rpm, 30 min	11	<2	0.14	18/20
ZnO _{ST} 2:2 w/w	3 g Zn(NO ₃) ₂ 6 g S 650 rpm, 15 min	15	<2	0.14	23/26
ZnO _{AG} 1:2 w/w	0.127 g Zn(NO ₃) ₂ 0.254 g AG, 350 rpm, 30 min	15	2.1	0.32	47/ca.50 ^c

^aS_{BET}: specific surface area was calculated by the Brunauer-Emmett-Teller (BET) equation; ^bD_{BJH}: mean pore size diameter was calculated by the Barret-Joyner Halenda (BJH) equation; ^cV_{BJH}: pore volumes were calculated by the Barret-Joyner Halenda (BJH) equation; ^dXRD NP sizes were calculated by the Scherrer equation. TEM NP sizes were worked out from TEM images averaging 15-20 particles. ^eAverage size 50 nm, some small nanocrystals (see TEM) could be observed.

Interestingly, alginic acid biotemplated nanocrystals were observed to have lower NP sizes as compared to starch and ex. agar materials. These results are in good agreement with previous reports from the group on the exceptional capping ability of alginic acid as compared to other polysaccharides in the preparation of nanomaterials.³⁵ Table 3 summarizes a comparison between the syntheses of ZnO nanomaterials from various polysaccharides, evidencing remarkably improved textural properties for the case of the extracted agar from macroalgae. Particularly, more than double pore volume and a narrower pore size (close to the mesoporous) was obtained in ex. agar biotemplated materials (ZnO_{AG}). XRD patterns of ZnO nanomaterials have been included in Figure 1 (see also ESI for all samples). Differences between samples were evidenced both in terms of crystallinity and phases present (particularly for ZnO_{AG} synthesized from ex. agar).

All nanomaterials exhibited the typical diffraction lines of ZnO hexagonal phase (zincite, P63mc) at 31.1° (100), 34.4° (002), 36.2° (101), 47.6° (102), 56.6° (110), 63°

(103) and minor 66° , 67.9° and 69° , in good agreement with previously reported literature results.³⁶ However, a significant variation in crystallinity was observed in the materials towards low crystalline samples at larger polysaccharide contents (e.g. 1:2 vs 1:8 mass ratios, Fig. 1B and D). As expected, milling was found to have a certain influence on the degree of crystallinity of the materials in good agreement with previous reports,^{33, 37} but this was not very significant at the relatively short milling times investigated in this work.

Interestingly, the polysaccharide mediated ZnO materials generally exhibited a rather pure ZnO diffraction pattern without any observable diffraction lines corresponding to mixed C/O/Zn species. These findings confirm the efficient removal of the sacrificial template upon calcination even for the case of ex. agar derived materials (ZnO_{AG}, Fig. 1C). Nevertheless, apart from a lower crystallinity, ZnO_{AG} nanomaterials from ex. agar contained some additionally interesting diffraction lines (Fig. 1C). In particular, these were related to the presence of highly crystalline KCl (diffraction lines at 28.4° , 40.6° , 50.4° , 66.6° and 74°) and a potassium sodium sulfate $K_3Na(SO_4)_2$ salt (diffraction lines at 30.4° , 31.4° and 45°). Their presence is supposed to be correlated with the presence of traces of K and S in the extracted agar material as reported previously by Francavilla *et al.*³⁴

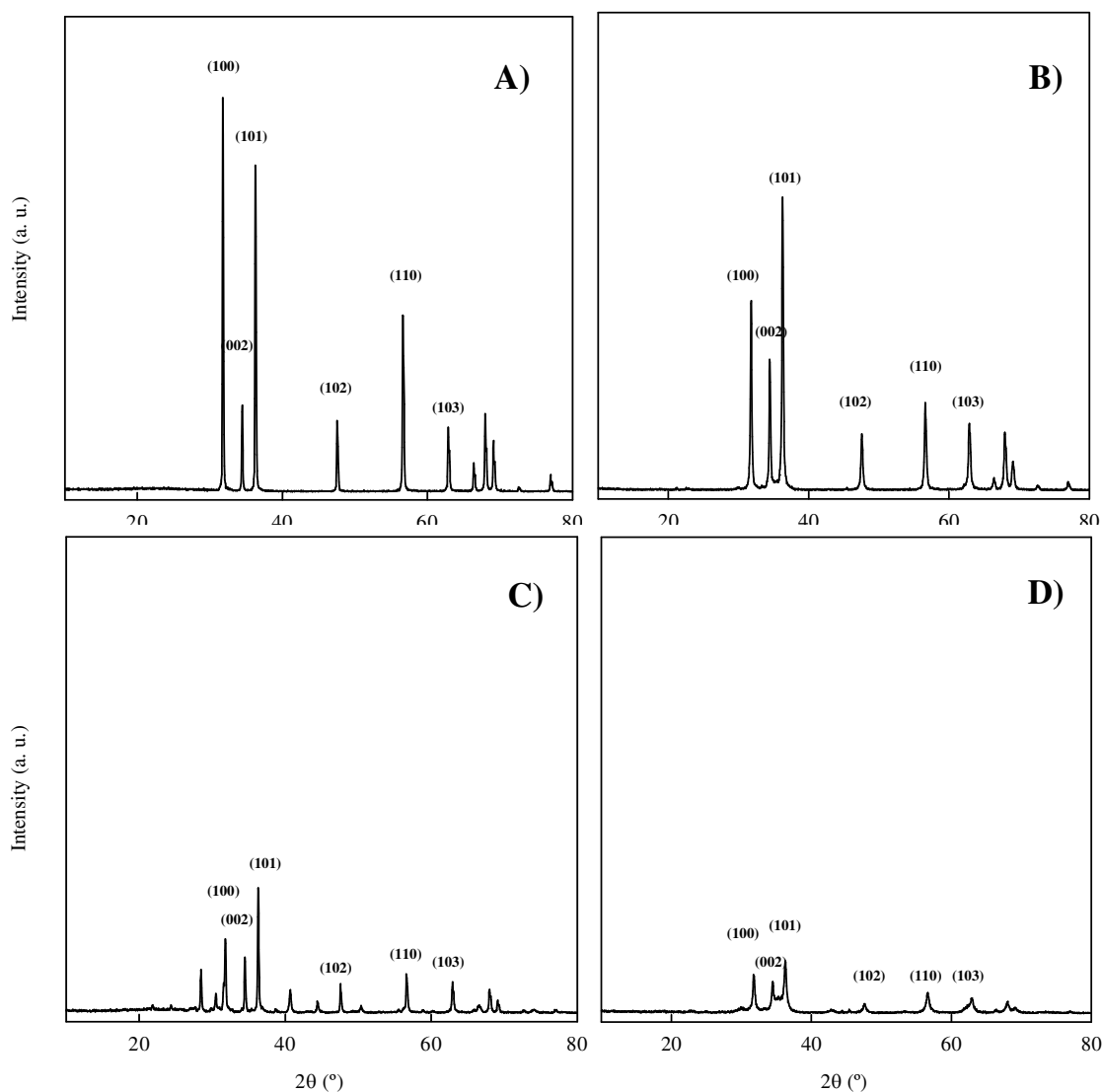


Fig. 1 XRD diffraction patterns of A) Reference crystalline ZnO_C; B) ZnO_{AA} 1.68 mmol g⁻¹ AA; C) ZnO_{AG} 1.68 mmol g⁻¹ AG; D) ZnO_{AA} 0.42 mmol g⁻¹ AA.

Representative TG-DTA profiles of the uncalcined milled Zn precursor/polysaccharide for the particular case of ex. agar from *Gracilaria* have been included in Fig. 2. A significant mass loss (over 35 wt%) was observed under 200°C, accompanied by a typical endothermic peak (due to physisorbed water before 100°C) as well as a sharp exothermic peak at 108-110°C (beginning of the decomposition step of

the organics from the agar polysaccharide). An even larger mass loss, accounting for ca. 50 wt.% of the total initial mass of sample, was clearly visible in the 120 to 490°C range, corresponding to the removal of the corresponding organic part of the polysaccharide. An intense exothermic peak was recorded centred at 382°C. Calcination of the material at temperatures above 500°C ensures in principle an almost complete removal of the polysaccharides from the material. Thus a temperature of 600°C selected for materials calcination seemed to be most appropriate. However, experimental data on impurities present in polysaccharide biotemplated materials (Table 4, see also ESI for other samples) indicate the presence of minor quantities of C in ZnO nanomaterials as well as other impurities in the case of ex. agar.

Table 4 Impurities present in ZnO_{AG} 1: 2 ex. agar nanomaterials upon calcination as determined by EDX^a

Element	wt.%	Atomic %
C	5.0	12.5
S	2.5	2.5
Ca	3.5	2.8
Al	1.8	2.0
Si	4.5	5.5
Cl	3.0	3.0

^a Averaging 4 measurements (four different domains of the sample)

The remarkable differences observed between samples were confirmed by SEM and TEM. SEM micrographs included in Figure 3 showcase unexpected differences in terms of morphology for ZnO nanostructures. The direct calcination of the metal precursor in the absence of polymer (ZnO_C) gave an expected random chunk-like

morphology, with large particle sizes (50-100 μm , Fig. 3A). Comparably, polymer biotemplated ZnO materials (ZnO_{AA} , ZnO_{AG} and ZnO_{ST}) depicted in Figures 3B to D exhibited different morphologies from flower-like for alginic acid and starch biotemplated ZnO (ZnO_{AA} and ZnO_{ST}) to a remarkable and perfectly arranged hexagonal-like shape for macroalgal-agar derived materials of ca. 1-5 μm (ZnO_{AG} , Fig. 3C inset). Such morphology was in good agreement with XRD results which indicated the presence of a P63mc hexagonal crystalline phase.

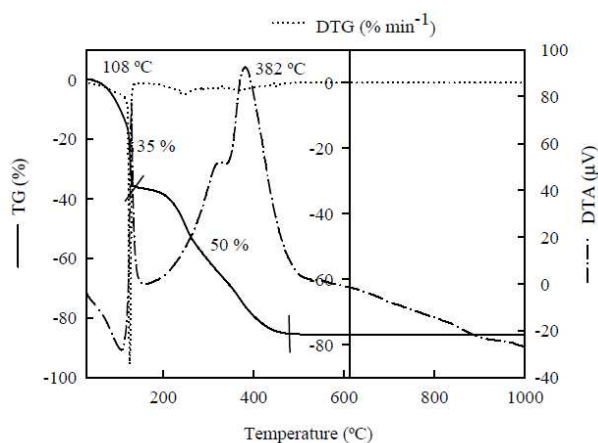


Fig. 2 TG-DTA profiles of sample ZnO_{AG} 1:2 ex. agar.

To the best of our knowledge, this is the first example of the synthesis of crystalline porous ZnO nanostructures based on a simple solid state grinding of metal precursors and pre-formed support consisting of a naturally extracted biopolymer from biomass (macroalga *Gracilaria gracilis*). Previous studies reported the use of agarose (purified agar) as soft template for synthesis of metal oxides (SiO_2 , TiO_2 , ZrO_2)²⁶⁻²⁷ as well as metal-oxides composites (TiO_2 -Au)²⁸. However, several synthetic steps including sol-gel processes, chemical reduction and solvothermal steps are generally involved in those methodologies as compared to the one-pot solventless

mechanochemical synthesis reported in this work. Furthermore, no direct agarose templated ZnO synthesis has been reported yet.

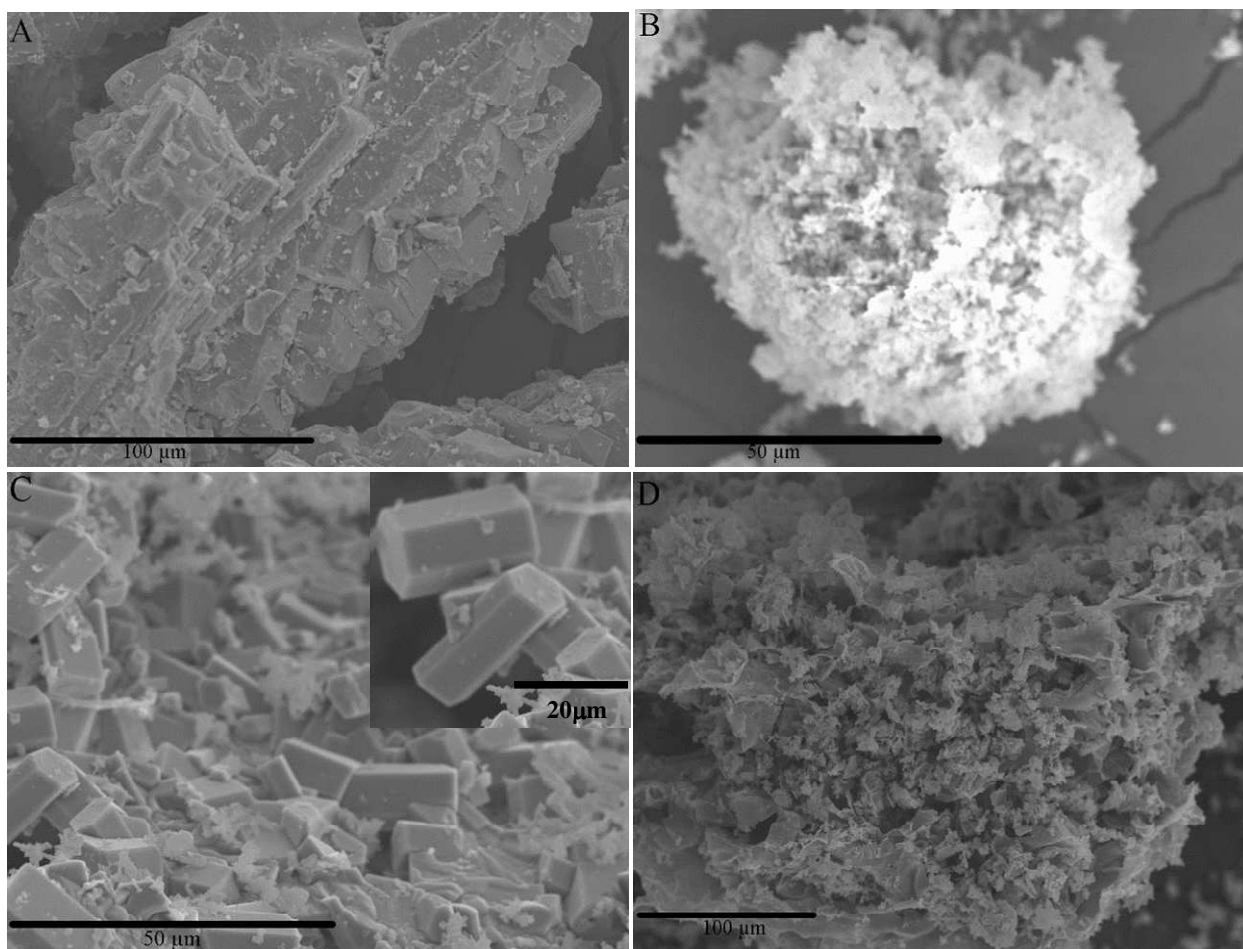


Fig. 3 SEM micrographs of A) ZnO_C obtained via direct calcination of Zn(NO₃)₂; B) bio-templated ZnO_{AA} nanocrystals using pure alginic acid; C) bio-templated ZnO_{AG} nanocrystals using macroalgae extracted agar; D) bio-templated ZnO_{ST} nanocrystals using pure starch.

The crystalline structure of ZnO materials as well as observed morphological changes were demonstrated by TEM measurements (Fig. 4). As compared to a rather continuous crystalline structure of non porous directly calcined ZnO (ZnO_C, Fig. 4A),

biotemplated ZnO materials exhibited a structure comprising small nanoparticle aggregates (ca. 5-10 nm) with NP sizes in the 25-50 nm depending on the material.

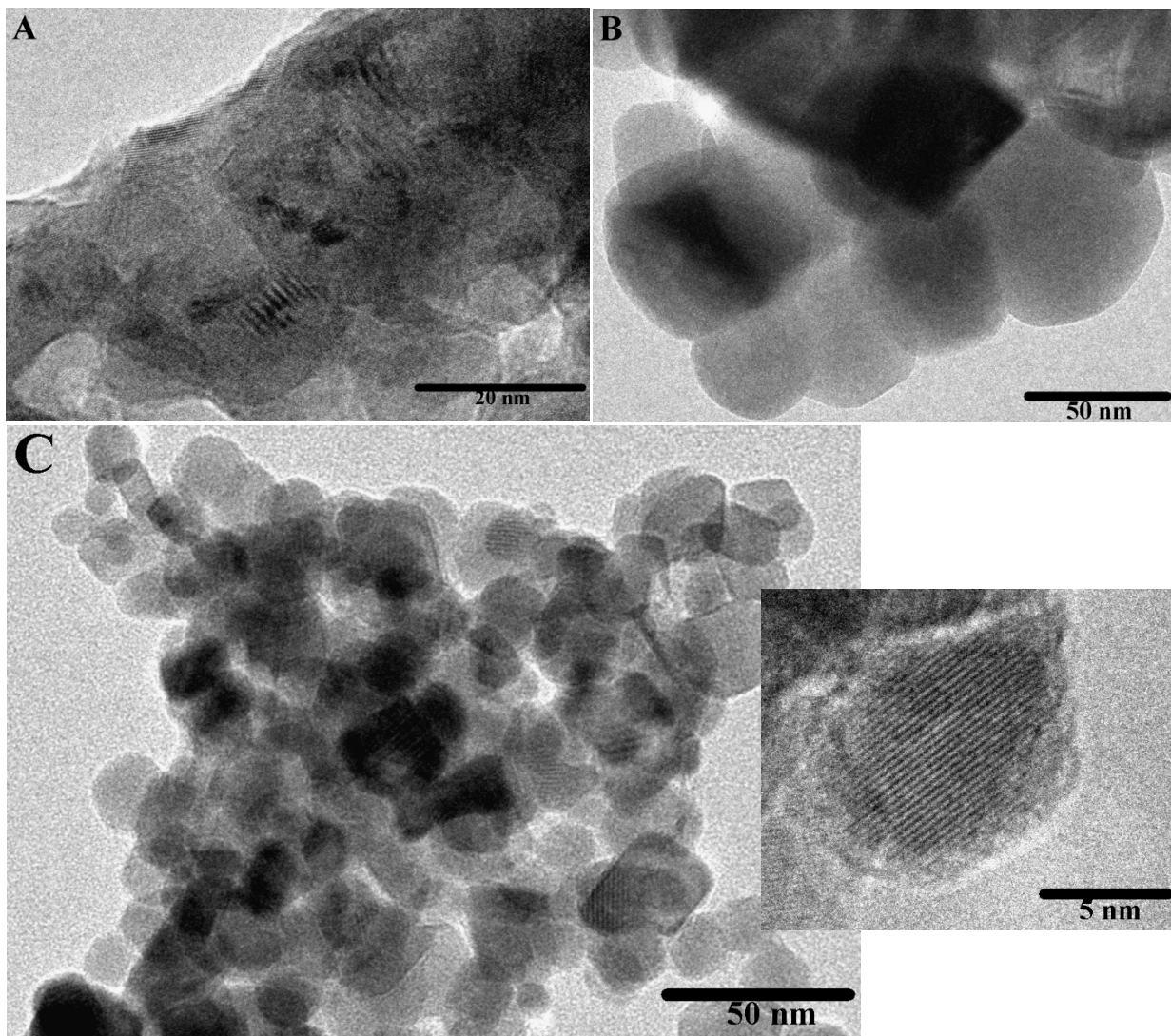


Fig. 4 TEM micrographs of A) non porous directly calcined ZnO_C; B) Alginic acid bio-templated ZnO_{AA} 1:2 precursor/polysaccharide mass ratio; C) ex. agar bio-templated ZnO_{AG} 1:2 precursor/polysaccharide mass ratio. Inset on C represents a High Resolution TEM image of a single nanocrystal from ex. agar synthesized ZnO_{AG}.

A high crystallinity was observed for most ZnO materials (see HR image in inset from Figure 4, also ESI for full details). Interestingly, increasing the quantity of polysaccharide in the mixture led to a mixture of nanoparticle and nanotubular-like nanostructures observed at large polysaccharide contents which can be related to the linear helical structure of polysaccharides such as starch (Fig. 5, see also ESI).

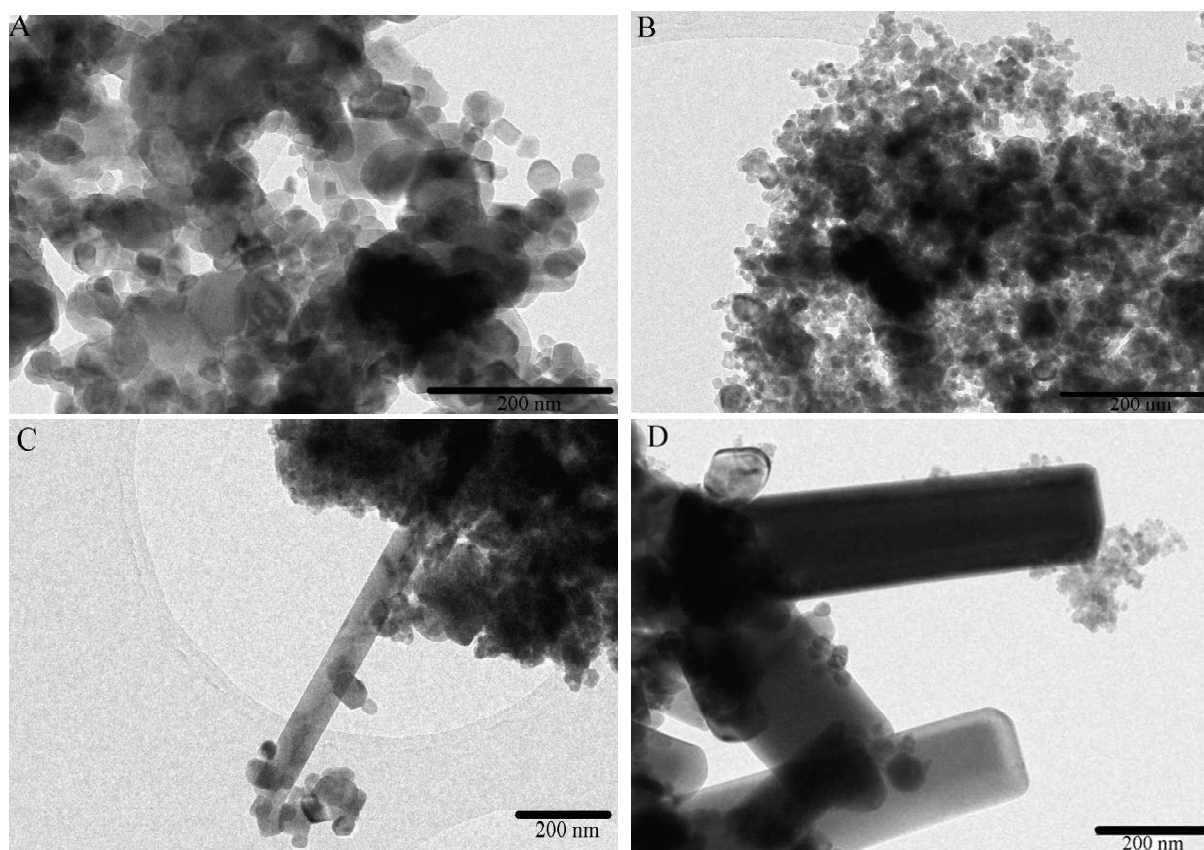


Fig. 5 Evolution of the nanostructures with changing precursor/polysaccharide mass ratios. A) $\text{Zn}(\text{NO}_3)_2$: alginic acid 1:1 w/w; B) $\text{Zn}(\text{NO}_3)_2$: alginic acid 1:2 w/w; C) $\text{Zn}(\text{NO}_3)_2$: alginic acid 1:4 w/w; D) $\text{Zn}(\text{NO}_3)_2$: alginic acid 1:8 w/w.

Based on these results, the presence of significant quantities of impurities in ex. agar biotemplated ZnO nanostructures and their potential implications in photocatalytic applications, the performance of two representative materials, namely ex. agar

synthesized ZnO_{AG} and alginic acid synthesized ZnO_{AA} as compared to commercial P25 Evonik were investigated in the photocatalytic degradation of phenol in water.

Phenol degradation efficiency results for different materials are shown in Figures 6 and 7 as well as Table 5. A significantly improved efficiency for phenol degradation was observed for ZnO_{AG} 1:2 ex. agar, also very similar to that of ZnO nanomaterials containing a large excess of polysaccharide as template (e.g. ZnO_{AA} 1:16 alginic acid). After 240 min of irradiation, almost 52 % of phenol was degraded using the naturally agar biotemplated ZnO_{AG}, a significant difference as compared to ZnO_{AA} biotemplated with alginic acid (<35% phenol degradation). A remarkable difference was also observed with respect to P25 Evonik in which initial activity was better but then leveled off while those of ZnO nanomaterials increased with time.

Table 5. Apparent rate constant (k_{app}) of phenol degradation for the synthesized catalysts.

Catalyst	Band gap (eV)	NP size (XRD/TEM) ^a	After 20 min.		After 240 min.		Degradation (%) after 240 min.
			K	R ²	k	R ²	
ZnO _{AA} 1:16 AA	3.0	33/35	0.0049	0.9991	0.0018	0.9163	35
ZnO _{AG} 1:2 AG	2.8	47/50 ^b	0.0072	0.9804	0.0028	0.9373	52
P25 Evonik		- /21	0.0245	0.9950	From 20 min. to 240 min. of illumination		37
	3.2				0.0009	0.9780	

^aXRD NP sizes were calculated by the Scherrer equation. TEM NP sizes were worked out from TEM images averaging 15-20 particles. ^bAverage size 50 nm, some small nanocrystals (see TEM) could be observed. Band gap of commercial ZnO: 3.2 eV.

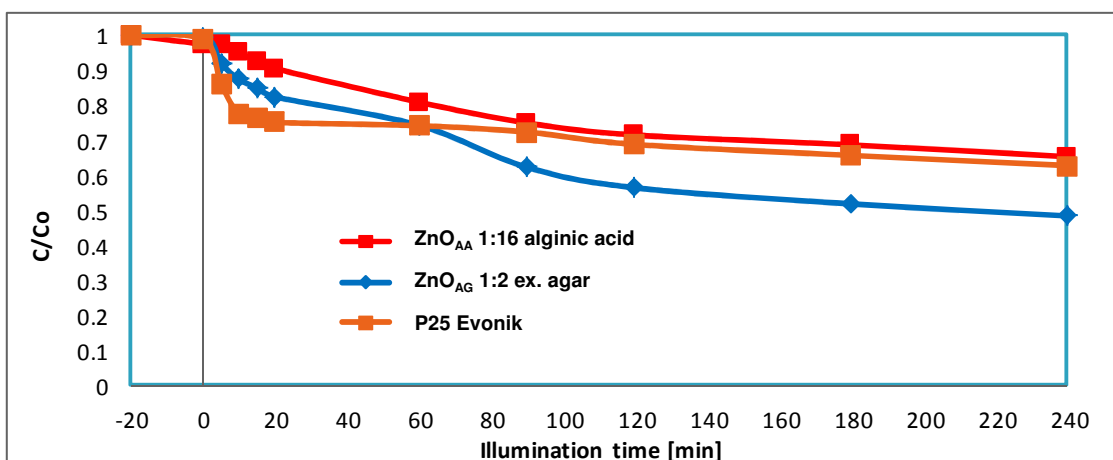


Fig. 6 Phenol degradation efficiency (measured as the relative concentration of phenol (C/C_0) over time) of ZnO_{AA} 1:16 alginic acid, ZnO_{AG} 1:2 ex. agar and P25 Evonik.

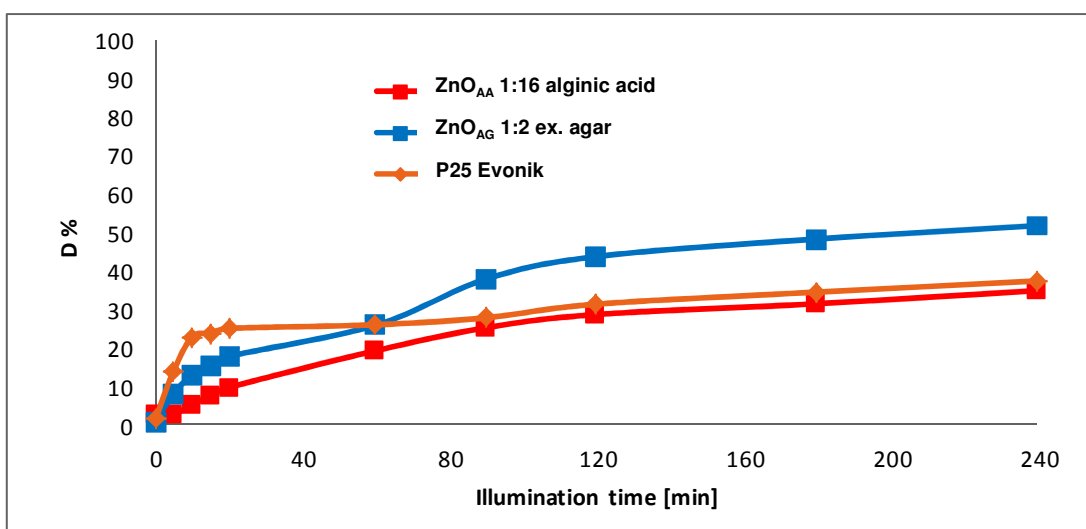


Fig. 7 Photocatalytic degradation curves of phenol for ZnO_{AA} 1:16 alginic acid, ZnO_{AG} 1:2 ex. agar and P25 Evonik.

On the basis of characterisation results and photocatalytic degradation findings, it seems like the presence of mainly C present in ZnO 1:2 ex. agar (as seen with a similar photocatalytic results obtained for ZnO 1:16 alginic acid containing ca. 8-10 wt.% C) can be correlated with the observed improved activity. While a decrease in band gap was noticeable in biotemplated ZnO nanocrystals as compared to P25 Evonik

and commercial ZnO (Table 5), no direct correlation between nanoparticle size and activity could be found from obtained data. In any case, additional synergetic effects of other impurities, namely S, metals and the determined salts or the increase in surface area of the materials cannot be ruled out as contributors to such improved photoactivity. Further investigations are currently ongoing in our laboratories to understand the contributions to the observed enhanced photocatalytic activities.

Conclusions

A simple and straightforward synthesis of porous ZnO nanostructures was efficiently conducted using a reactive milling protocol under mild conditions and short times of milling (typically 30 min) by using a range of polysaccharides as sacrificial templates including an extracted agar from macroalgae. The synthesized ZnO were found to be highly crystalline nanostructured materials, with a particularly promising photocatalytic phenol degradation demonstrated for the porous ZnO nanostructure prepared from extracted agar from the red macroalga *Gracilaria gracilis*. Due to its simplicity, wide applicability and reproducibility, the proposed protocol has an enormous potential and is envisaged to pave the way to the synthesis of various porous nanostructures of different metal oxides (e.g. iron oxides, TiO₂, Al₂O₃, CeO₂, etc.) currently under investigation in our laboratories. Nevertheless, the economic and environmental credentials of the proposed solid state milling process as compared with “conventional” synthesis will be part of future investigations of the group.

Acknowledgments

RL gratefully acknowledges Ministerio de Ciencia e Innovación, Gobierno de España for the concession of a Ramon y Cajal contract (ref. RYC-2009-04199) and funding

under project CTQ2011-28954-C02-02 as well as Consejería de Ciencia e Innovación, Junta de Andalucía for funding under project P10-FQM-6711. Matteo Francavilla gratefully acknowledges the European Commission, Directorate-General for Research & Innovation, for funding the project “STAR*AgroEnergy” (FP7 Regpot 2011-1, Grant Agreement N° 286269).

References

- 1 N. Huebsch and D. J. Mooney, *Nature* 2009, **462**, 426-432.
- 2 J. W.-H. Li and J. C. Vederas, *Science* 2009, **325**, 161-165.
- 3 J. M. Patete, X. Peng, C. Koenigsmann, Y. Xu, B. Karn and S. S. Wong, *Green Chem.* 2011, **13**, 482-519.
- 4 M. Epifani, J. Arbiol, R. Díaz, M. J. Perálvarez, P. Siciliano and J. R. Morante, *Chem. Mater.* 2005, **17**, 6468-6472.
- 5 S. Labuayai, V. Promarak and S. Maensiri, *Appl. Phys. A* 2009, **94**, 755-761.
- 6 L. Spanhel and M. A Anderson, *J. Am. Chem. Soc.* 1991, **113**, 2826-2833.
- 7 E. A. Meulenkamp, *J. Phys. Chem. B* 1998, **102**, 5566.
- 8 C. L Carnes and K. J. Klabunde, *Langmuir* 2000, **16**, 3764-3772.
- 9 R. M. Nyffenegger, B. Craft, M. Shaaban, S. Gorer, G. Erley and R. M. Penner, *Chem. Mater.* 1998, **10**, 1120-1129.
- 10 J. Hu, M. Chen, X. Fanga and L. Wu *Chem. Soc. Rev.* 2011, **40**, 5472–5491.
- 11 H. Cong and S. Yu *Adv. Funct. Mater.* 2007, **17**, 1814-1820.
- 12 J. Zhang, J. Wang, S. Zhou, K. Duan, B. Feng, J. Weng, H. Tang and P. Wu *J. Mater. Chem.* 2010, **20**, 9798–9804.
- 13 W. Wang, L. Wang, L. Liu, C. He, J. Tan and Y. Liang, *Cryst. Eng. Commun.* 2012, **14**, 4997–5004.

- 14 A. Taubert, D. Palms, O. Weiss, M-T. Piccini and D. N. Batchelder, *Chem. Mater.* 2002, **14**, 2594-2601.
- 15 M. C. Kimling and R. A. Caruso, *J. Mater. Chem.* 2012, **22**, 4073-4082.
- 16 J. Cai, S. Liu, J. Feng, S. Kimura, M. Wada, S. Kuga and L. Zhang, *Angew. Chem. Int. Ed.* 2012, **51**, 2076-2079.
- 17 P. Raveendran, J. Fu and S. L. Wallen, *Green Chem.* 2006, **8**, 34–38.
- 18 S. Chairam, C. Poolpermand, E. Somsook, *Carbohydr. Polym.* 2009, **75**, 694–704.
- 19 N. Vigneshwaran, R. P. Nachane, R. H. Balasubramanya and P. V. Varadarajan, *Carbohydr. Res.* 2006, **341**, 2012–2018.
- 20 D. K. Bozanic, V. Djokovic, J. Blanusa, P. S. Nair, M. K. Georges and T. Radhakrishnan, *Eur. Phys. J. E* 2007, **22**, 51–59.
- 21 A. El Kadib, K. Molvinger, T. Cacciaguerra, M. Bousmina and D. Brunel, *Microporous Mesoporous Mater.* 2011, **142**, 301-307.
- 22 P. Sipos, O. Berkesi, E. Tombacz, T. G. St Pierre and J. Webb, *J. Inorg. Biochem.* 2003, **95**, 55–63.
- 23 B. Wang, C. Tian, L. Wang, R. Wang and H. Fu, *Nanotechnol.* 2010, **21**, 025606.
- 24 M. J. Laudenslager, J. D. Schiffman and C. L. Schauer, *Biomacromolecules* 2008, **9**, 2682–2685.
- 25 K. F. Du, D. Yang and Y. Sun, *Ind. Eng. Chem. Res.* 2009, **48**, 755-762.
- 26 G. L. Drisko, X. Wang and R. A. Caruso, *Langmuir*, 2011, **27**, 2124-2127.
- 27 J. Zhou, M. Zhou and R. A. Caruso, *Langmuir*, 2006, **22**, 3332-3336.
- 28 X. Wang, T. Dornom, M. Blackford and R. A. Caruso, *J. Mater. Chem.* 2012, **22**, 11701-11710.

- 29 Z. Schnepf, S. R. Hall, M. J. Hollamby and S. Mann, *Green Chem.* 2011, **13**, 272-275.
- 30 Z. Schnepf, S. C. Wimbush, S. Mann, S. R. Hall, *CrystEngComm*, 2010, **12**, 1410–1415.
- 31 Y. Liu, J. Goebel and Y. Yin, *Chem. Soc. Rev.* 2013, **42**, 2610-2653.
- 32 H. Bai, F. Xu, L. Anjia and H. Matsui *Soft Matter*. 2009, **5**, 966–969.
- 33 A. Pineda, A.M. Balu, J.M. Campelo, A.A. Romero, D. Carmona, F. Balas, J. Santamaria and R. Luque, *ChemSusChem* 2011, **4**, 1561-1565.
- 34 M. Francavilla, A. Pineda, C.S.K. Lin, M. Franchi, P. Trotta, A.A Romero and R. Luque, *Carbohydr. Polym.* 2013, **92**, 1555– 1560.
- 35 R. Luque, R. Campos, A. Garcia, C. Lastres, M. Ojeda, A. Pineda, A.A. Romero and A. Yopez, *RSC Adv.* 2013, **3**, 7119-7123.
- 36 M. Monge, M.L. Kahn, A. Maisonnat and B. Chaudret, *Angew. Chem. Int. Ed.* 2003, **42**, 5321–5324.
- 37 a) M. Benoit, A. Rodrigues, K. de Oliveira Vigier, E. Fourré, J. Barrault, J.-M. Tatibouët and F. Jérôme, *Green Chem.* 2012, **14**, 2212-2215; b) R. Carrasquillo-Flores, M. Kaldstrom, F. Schuth, J.A. Dumesic and R. Rinaldi, *ACS Catal.* 2013, **3**, 993–997.